




Microstructures documenting Cenozoic extension processes in the northern continental margin of the South China Sea

Liheng Sun, Zhen Sun, Xiaolong Huang, Yingde Jiang & Joann Miriam Stock


To cite this article: Liheng Sun, Zhen Sun, Xiaolong Huang, Yingde Jiang & Joann Miriam Stock (2020) Microstructures documenting Cenozoic extension processes in the northern continental margin of the South China Sea, *International Geology Review*, 62:7-8, 1094-1107, DOI: [10.1080/00206814.2019.1669079](https://doi.org/10.1080/00206814.2019.1669079)

To link to this article: <https://doi.org/10.1080/00206814.2019.1669079>

 [View supplementary material](#) 



 Published online: 29 Sep 2019.

 [Submit your article to this journal](#) 

 Article views: 176

 [View related articles](#) 

 [View Crossmark data](#) 

 Citing articles: 2 [View citing articles](#) 

Microstructures documenting Cenozoic extension processes in the northern continental margin of the South China Sea

Liheng Sun^{a,b}, Zhen Sun^a, Xiaolong Huang^c, Yingde Jiang^c and Joann Miriam Stock^d

^aCAS Key Laboratory of Ocean and Marginal Sea Geology, South China Sea Institute of Oceanology, Chinese Academy of Sciences, Guangzhou, China; ^bCollege of Earth and Planetary Sciences, University of Chinese Academy of Sciences, Beijing, China; ^cState Key Laboratory of Isotope Geochemistry, Guangzhou Institute of Geochemistry, Chinese Academy of Sciences, Guangzhou, China; ^dDivision of Geological and Planetary Sciences, California Institute of Technology, Pasadena, CA, USA

ABSTRACT

In order to investigate the thinning process of the northern continental margin of the South China Sea, petrographic and microstructural analysis were carried out on 20 greenschist-facies mylonite samples, which were obtained from Site U1504 of IODP Expedition 367/368 in the Outer Margin High of the region. The mineral assemblage of the greenschist-facies mylonite is chlorite + epidote + albite (Ab = 94.7–99.9) + quartz, which contains 10–30% gravel components. Microstructural analysis indicates that the greenschist-facies mylonite experienced two episodes of deformation: early ductile deformation followed by a later stage of brittle deformation. Both episodes of deformation suggest an extensional environment. The extensive development of bulging recrystallization (BLG) of quartz, microscopic fractures and fine granulation of albite suggest that the temperature of ductile deformation is about 300–400°C, compatible with a ductile shearing at shallow crust levels (~5–10 km). Petrographic features suggest that the greenschist-facies mylonite might originate from volcanic sedimentary rocks or sedimentary rocks affected by the intrusion of mafic magma. Combined with seismic interpretation, we propose that the greenschist-facies mylonite might be formed by crustal exhumation after thick Mesozoic sediments were denuded by a major extension.

ARTICLE HISTORY

Received 4 March 2019
Accepted 14 September 2019

KEYWORDS

Greenschist-facies mylonite; petrography; microstructure; Continental margin of the northern South China Sea; Cenozoic; IODP367/368

1. Introduction

The South China Sea (SCS) is one of the largest marginal seas in the western Pacific. Onland and offshore outcrops suggested that the SCS region has suffered overlapping effects from Pacific subduction and Tethys tectonic regime during Paleozoic to Mesozoic (Zhou and Li 2000; Li *et al.* 2012b). The Cenozoic rifting and spreading occurred at an oblique angle to the Mesozoic subduction system (Li *et al.* 2018). Thus, although classified as a passive continental margin in nature (Taylor and Hayes 1983), the northern continental margin of the SCS is different from the Iberian and Newfoundland margins (Sutra and Manatschal 2012; Sutra *et al.* 2013) in many aspects, such as the inherited basement petrological composition, more rapid transition from continental rifting to seafloor spreading (Larsen *et al.*, 2018), and the newly developed mainly landward-dipping fault systems.

In order to reveal the thinning process of the SCS, IODP Expeditions 367, 368 and 368X drilled seven sites from the Continent–Ocean Transition (COT) zone to the early ocean of the SCS in 2017 and 2018 (Sun *et al.*

2018; Childress *et al.*, 2019). Altered basalt was recovered at U1502, within the region that was conjectured to be the COT (Sun *et al.* 2016). Larsen *et al.* (2018) concluded that the SCS is different from the Iberia and Newfoundland margins, because the rifting to early break-up stage of the SCS should have involved more magma. For the first time, scientists encountered mafic greenschist facies mylonite in the basement of the Outer Margin High (OMH). Above the mylonite, early syn-rift and pre-rift strata (comprising sandstone with gravels at site U1501) are missing; instead, late Eocene and younger sediments are directly in contact with the basement metamorphic rocks (Sun *et al.* 2018).

The northern continental margin of the South China Sea has completely retained the products of the passive continental margin in the process of extension, thinning and rupture, making it an ideal place to study the formation and evolution of passive continental margins (Zhou 2018). Due to technical limitations, the previous studies on the tectonic characteristics of the northern continental margin of the South China Sea were mainly conducted by geophysical methods (Sun *et al.* 2016,

2018). However, the acquisition of greenschist facies mylonite in the COT provides a new data set to constrain the tectonic movement of the northern continental margin of the South China Sea. Located in the COT of the northern continental margin, the greenschist facies mylonite may preserve important information about Cenozoic rifting and thinning processes, or even Mesozoic subduction history. In this paper, petrography, mineral chemistry and microstructure analysis on greenschist facies mylonite were carried out to extract this information. Combined with seismic profile interpretation, we also discuss the tectonic processes in the SCS.

2. Geological setting

The northern SCS margin is bounded by the Manila subduction zone to the east, the central and the north-west sub sea basin to the south, and the Indosinian block to the west (Figure 2).

In the Mesozoic, the northern margin of the SCS lay above the subducting Izanagi plate; the region then transitioned into a passive continental margin from late Cretaceous to early Eocene time (Li *et al.* 2012a; Yao 1996; Zhang 2012; Seton *et al.* 2015). In Cenozoic time, the northern margin of the SCS experienced intense crustal thinning, which then developed into an ocean after late Oligocene time. Through multiple stages of extension, a large number of highly extended

rifted basins controlled by detachment faults developed (Ren *et al.* 2015, Sun *et al.* 2016, 2018).

Site U1504 is located in the southeast of the Pearl River Mouth basin, where there are several basement highs trending NE (Figure 1(c)) collectively named the Outer Margin High (OMH) (Sun *et al.* 2016). U1504 sits at the shoulder of one basement high on the OMH (Sun *et al.* 2018). The evolution of the Pearl River Mouth basin, where the greenschist mylonite is located, can be summarized into four main stages: (1) The active marginal stage in the late Mesozoic (middle Jurassic – late Cretaceous time) characterized by low-angle subduction of the Izanagi/Pacific plate; (2) the rifting stage, from late Cretaceous to Eocene time, featured by a series of NE-oriented rift basins; (3) the seafloor spreading stage from Oligocene to middle Miocene time; (4) a post-spreading subduction stage after the middle Miocene, in which the SCS basin began to narrow due to subduction of the SCS crust at the Manila trench (Luan and Zhang 2009; Wang 2012).

3. Samples and methods

3.1. Samples

In U1504, there are two holes, U1504A and U1504B (Figure 2). The distance between the two holes is around 200 m. From top to bottom, both holes U1504A and U1504B can be divided into three parts, with the top and middle parts composed of abyssal and

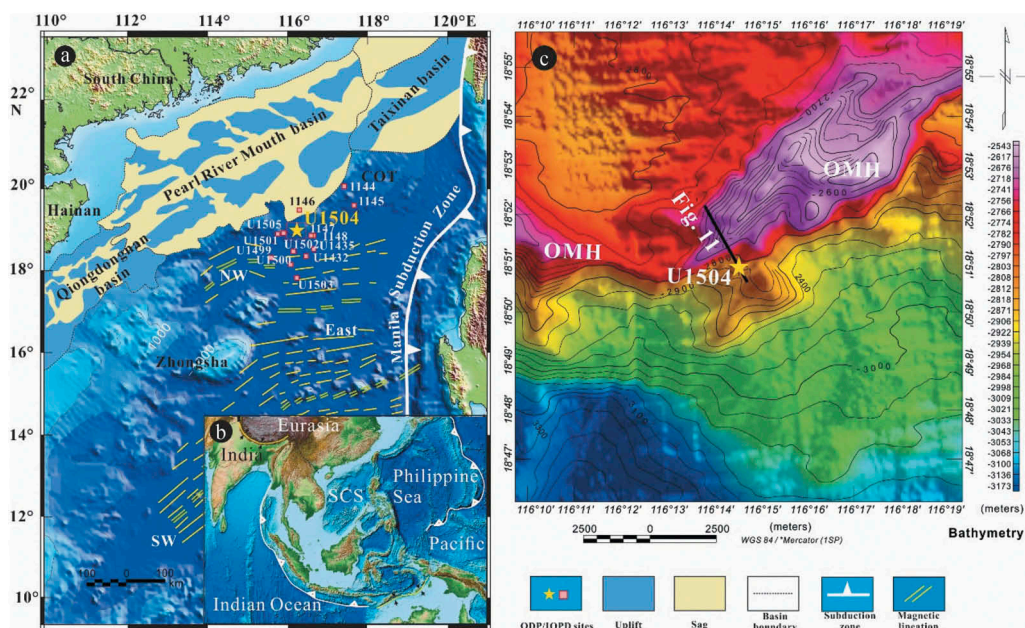


Figure 1. Bathymetric map of the South China Sea (a) and site location (c). The insert figure in the lower right corner (b) is the geotectonic background map. The yellow pentagram is site location for U1504. Abbreviations of tectonic units in the study area: COT – Continent-Ocean transition zone; SCS – South China Sea; OMH-Outer Margin High.

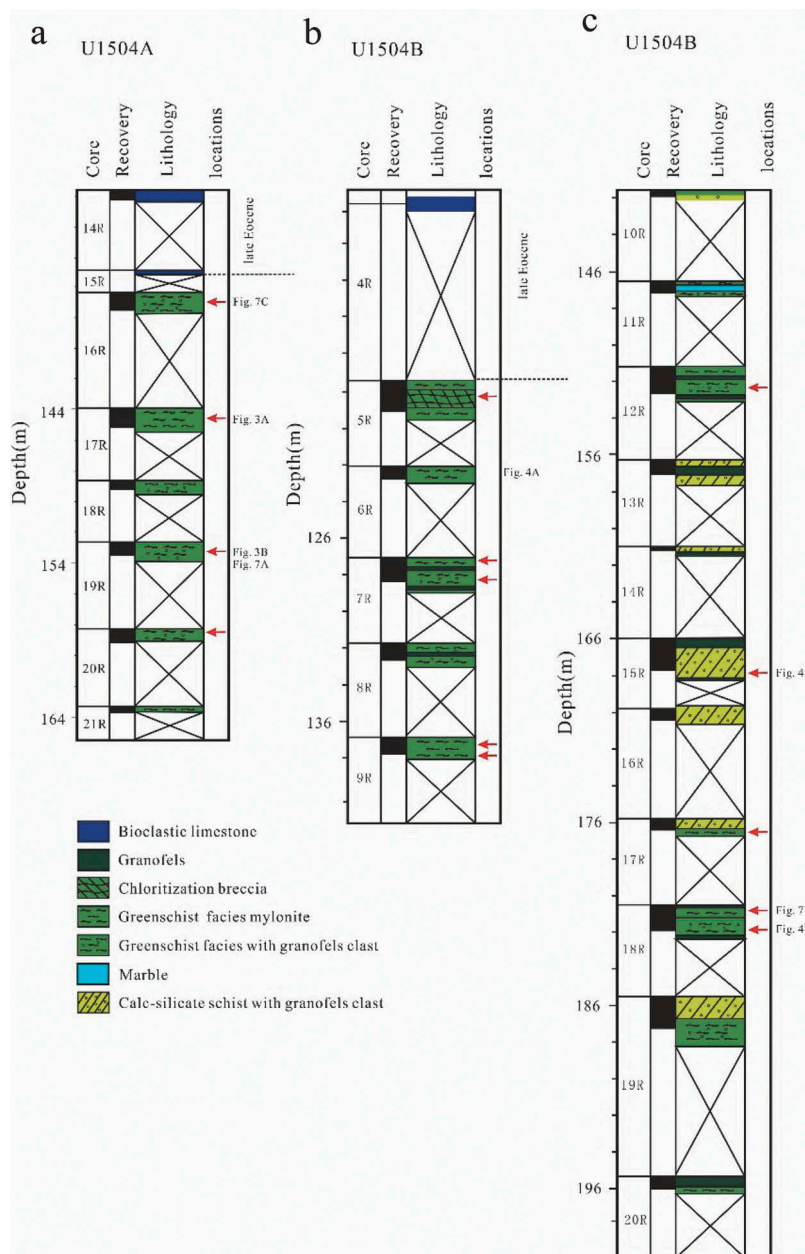


Figure 2. Lithostratigraphic summary of the metamorphic rocks in Hole A (a) and Hole B (b, c) of Site U1504. Metamorphic rocks of U1504A is mainly greenschist facies mylonite. The upper part of the metamorphic rocks of U1504B is dominated by chloritic breccia and greenschist facies mylonite with clast, and the lower part is dominated by greenschist facies mylonite. The red arrows mean locations of samples analysed.

hemipelagic sediments. The lowest part is basic metamorphic rocks, including greenschist facies mylonite and calc-silicate schist. Late Eocene and younger sediments directly overlie the metamorphic rock. The samples of this study were collected from the lower part of Site U1504. Metamorphic rocks are found in U1504A at 136.4–163.7 m, and in U1504B at 117.4–196.3 m. Metamorphic rocks of U1504A are mainly greenschist facies mylonite (Figure 3): the upper part of the metamorphic rocks of U1504B are dominated by chloritic breccia and greenschist facies mylonite with clasts,

and the lower part is dominated by greenschist facies mylonite (Figure 4).

3.2 Methods

3.2.1. Petrography and microstructure analysis

The preliminary preparation for the samples was completed in the Key Laboratory of Ocean and Marginal Sea Geology, South China Sea Institute of Oceanology, including numbering, cleaning, drying and identification. The oriented thin sections were prepared by Guangzhou

Tuoyan Testing technology co. LTD. The identification of thin sections, in the Polarizing Microscope Laboratory, Guangzhou Institute of Geochemistry, Chinese Academy of Sciences, included microstructure and mineral composition analysis. Thin sections were cut along vertical foliation and parallel to lineation, on which top direction was marked.

3.2.2. Seismic profile

Seismic profiles across U1504 were collected by CNOOC in 2015 using a 6 km streamer (480 channels) and moderately-sized, tuned, airgun arrays (4100 cu. in.). Sample intervals are 1 ms, and broad recording bandwidth (open low-cut and up to 400 Hz high-cut filters) is utilized. The primary processing flow emphasized multiple attenuation and pre-stack time migration. The CDP interval is 6.25 m. Sequences were marked according to the microfossil identification of Expeditions 367/368 (Sun *et al.* 2018) and correlation with neighbouring lines.

3.2.3. Mineral chemistry analysing

Mineral compositions analyses were carried out using a JEOL JXA-8100 electron microprobe (EPMA) at the State Key Laboratory of Isotope Geochemistry, Guangzhou Institute of Geochemistry, Chinese Academy of Sciences, with the operating conditions of 15 kV accelerated voltage, 20 nA beam current, 1 μm beam size, and a ZAF correction procedure for data reduction. The analytical errors are less than 0.45%.

4. Petrography

4.1. U1504A

Greenschist facies mylonite in U1504A (Figure 3) is mainly composed of chlorite ($\text{SiO}_2 = 26.99\text{--}28.16$ wt%; $\text{MgO} = 14.17\text{--}15.35$ wt%; $\text{FeO} = 25.97\text{--}28.38$ wt%), epidote ($\text{SiO}_2 = 36.57\text{--}41.73$ wt%; $\text{CaO} = 19.42\text{--}23.28$ wt%; $\text{FeO} = 5.12\text{--}15.43$ wt%), albite ($\text{Ab} = 94.7\text{--}99.9$), quartz and other minerals, including a small amount of pyroxene (Supplementary Table 5). Albite and quartz are mostly in veins or gravels. The veins mainly exist in clasts in the gravels and occasionally extend into the matrix. The sample contains 10–15% angular to rounded clasts as large as 6 cm. Small clasts are usually rotated into alignment with the foliation, while large clasts show no preferred orientation. The clasts have generally isotropic textures with only a weakly developed foliation. The clasts are mainly felsic or mafic igneous rocks, which preserve a lot of minerals of the protolith, which will aid in the discrimination of their

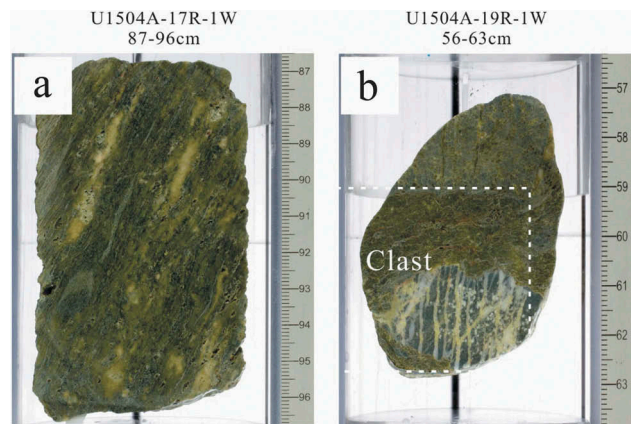


Figure 3. Photos of U1504A metamorphic rocks.

A: Greenschist-facies mylonite, oriented metamorphic minerals and gravels mainly define mylonite foliation, the latter developed a steep angle of about 40–50°; B: Greenschist facies mylonite with clasts. In the clast, a large number of veins developed and did not extend outside to the matrix.

protolith composition. The mafic igneous gravels have a mineral assemblage of albite + pyroxene. The felsic gravels have a mineral assemblage of albite + quartz. Most quartz crystals exhibit the features of dynamic recrystallization, while some albite crystals show sodium zoisitization and fine granulation to form an aggregate of epidote (Figure 5(a)). The metamorphic mineral assemblage of greenschist facies mylonite with clasts is chlorite + epidote + albite + quartz. Because of the lack of high temperature metamorphic minerals, the gravels are classified as a greenschist facies mylonite.

4.1. U1504B

According to observed mineral compositions, U1504B is composed of two units, chloritic breccia and greenschist mylonite. Chloritic breccia is mostly identified in the upper part of the basement core, while greenschist facies mylonite is mostly found in the lower part. With increasing depth, the chloritic breccia gradually transforms into greenschist facies mylonite. Since greenschist mylonite in U1504B is very similar to that of U1504A in both mineral composition and microstructure, this section mainly describes the mineral composition and microstructure characteristics of the chloritic breccia.

The chloritic breccia is mainly composed of chlorite ($\text{SiO}_2 = 27.24$ wt%; $\text{MgO} = 15.58$ wt%; $\text{FeO} = 26.08$ wt%), epidote ($\text{SiO}_2 = 32.87\text{--}38.09$ wt%; $\text{CaO} = 14.40\text{--}23.14$ wt%; $\text{FeO} = 5.07\text{--}14.03$ wt%), albite ($\text{Ab} = 95.1\text{--}99.2\%$), quartz, and a small amount of pyroxene ($\text{Wo}_{42.3\text{--}45.4}$ $\text{En}_{27.4\text{--}44.0}$ $\text{Fs}_{23.5\text{--}11.5}$), sericite, and calcite (Figure 5(b)) (Supplementary Table 5). Albite and quartz occur mostly in the veins and clasts as fine-grained crystals. The Albite

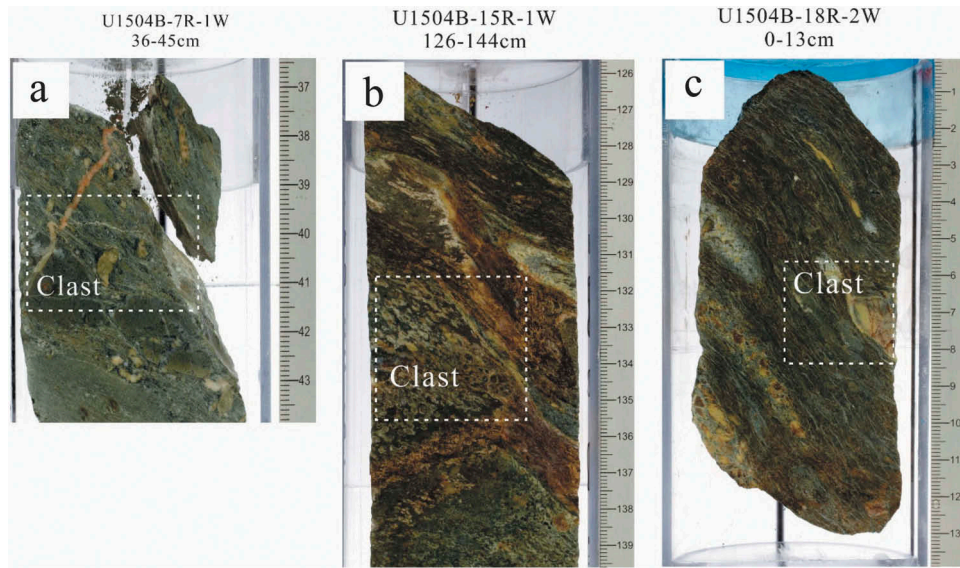


Figure 4. Photos of U1504B metamorphic rocks.

(a, c): Greenschist-facies mylonite with clast, which is very similar to that of U1504A in both mineral composition and microstructure; (b): Chloritic breccia, the chloritic breccia has weak foliation, with oriented metamorphic minerals and clasts defining the foliation. Compared to U1504A, chloritic breccia contains more clasts with irregular shapes and complex compositions.

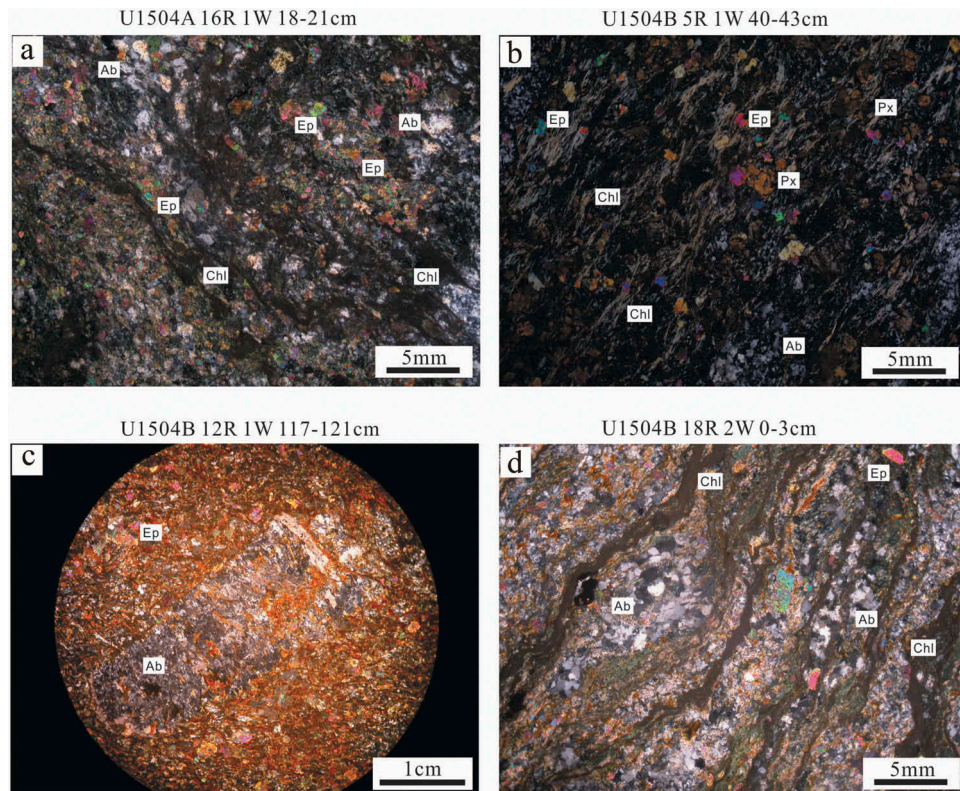


Figure 5. Mineral assemblage in metamorphic rocks under the microscope.

(a): Albite occurs with sodium zoisitization and fine granulation, which formed an aggregate of epidote; (b): Metamorphic mineral assemblage of chloritic breccia; (c): Some of the albite have complete and clearly defined crystals, but with internal dissolution, showing residual dissolution structure; (d): Albite occurs with sodium zoisitization; fine granulation with oriented metamorphic minerals and clasts defining the mylonite foliation. Ab- albite; Ep- epidote; Chl- chlorite; Px- pyroxenes. These abbreviations have the same meaning in the subsequent figures.

has a complete crystal shape with a clear outline, but internal dissolution was observed, indicating a residual dissolution structure (Figure 5(c)). Calcite occurs as individual crystals and veins. Some calcite veins cut through both clasts and mylonites, suggesting a relatively late formation. Compared with U1504A, chloritic breccia contains more clasts with irregular shapes and complex compositions. The clasts have a low degree of metamorphism and slight internal deformation, which preserves the mineral assemblage of the protolith quite well.

5. Microstructure

5.1. Microstructure deformation and period

According to the petrographic characteristics, the mylonite foliation in the studied samples is the most direct evidence of ductile deformation (Figure 6(a)). Greenschist-facies mylonite with clasts usually shows strong foliation. The preserved foliation is quite steep, with dipping angles varying from 50–60° to vertical, mostly reaching 70°, and decreasing from shallow to deep. Metamorphic minerals are oriented along the mylonitic planes, and show the growth around clasts. Accordingly, these oriented minerals and clasts jointly define the mylonitic plane (Figure 5(a,b,d)). S-C fabric, asymmetric rotational augen and intrafolial folds are observed in places, which indicate that the foliation is affected by a normal shearing motion (Figure 7). The chloritic breccia also has a weak foliation, defined by oriented metamorphic minerals and clasts. The asymmetric rotational augens and intrafolial folds in such rock also indicate that the formation of the foliation is related to a normal shearing motion, similar to that described in Hole U1504A (Figure 7).

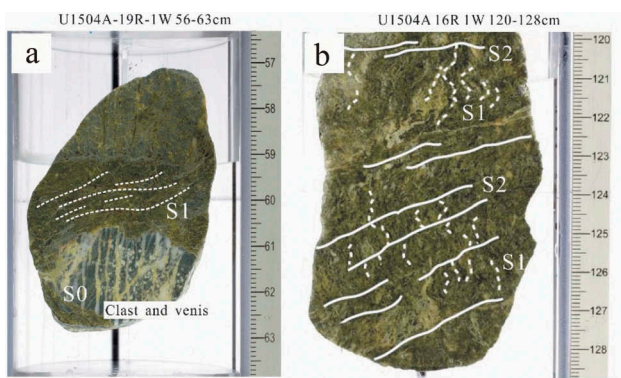


Figure 6. Schematic diagram of deformation periods.

A: The early stage of ductile shear movement formed a widely developed mylonitic foliation, which surrounds the clast. B: The compaction foliation is transformed by fold cleavage, which indicates that the rock underwent another brittle deformation in the late stage. S0: Protolith; S1: Mylonitic foliation; S2: fold cleavage.

In the upper part of greenschist-facies mylonitic in Holes U1504A and U1504B, weak crenulation cleavage, fractures, and calcite veins were observed cutting through the foliation, suggesting a more recent phase of brittle deformation (Figure 6(b)). In over 30 samples, fold cleavages, fissures and calcite veins show a high dip angle relative to the core axis of about 40° to 60°, ranging occasionally up to nearly vertical. Under the microscope, the felsic clasts are transformed and fractured along the direction nearly perpendicular to the foliation, which was consistent with the results of observations of hand specimens.

Accordingly, two episodes of deformation can be identified for the greenschist samples; the early episode is characterized by a strong ductile deformation in the brittle-ductile transition zone of the crust, forming well-developed mylonitic foliation (Figure 6(a)). The later episode developed at a shallow crustal level, which led to the formation of fragmentation structure and brittle cleavages (Figure 6(b)). Microstructures in both stages show an extensional environment with the early ductile deformation stage being the main deformation stage.

5.2. Microstructure of feldspar and quartz

Eighteen pieces of thin sections were selected to study the microstructures of feldspathic granules and veins that are parallel to mylonitic foliation.

The recrystallization of quartz forced the former crystal boundaries to expand towards areas with high dislocation density, so that bulging recrystallization (BLG) was observed. The recrystallized grains are nearly equal in size, surrounding the original grains or inside the original grain cracks. The large quartz grains usually contain deformation zones, deformation twins and wavy extinction. Recrystallized quartz grains from the BLG zone are slightly elongated (ratio < 1:3) with a preferred orientation parallel to foliation, and have an irregular shape with serrated boundaries (0.1–0.5mm) (Figure 8(a)). Some other recrystallized quartz grains developed along the periphery or within fissures of albite, forming an alteration zone around the albite grain (Figure 8(d)). The dominant microstructural features of the studied samples include BLG for quartz; however, SGR (subgrain rotation recrystallization) is locally present (Figure 8(a,d)). The typical microstructure of SGR is represented by highly elongated quartz grains (ratio > 1:5). These deformation styles are typical of medium to low temperature metamorphism, in which the mobility of quartz grain boundaries is limited (Frederico *et al.* 2010).

The residual feldspar crystals are often elongated and strongly fractured, and the fracture is filled with fine

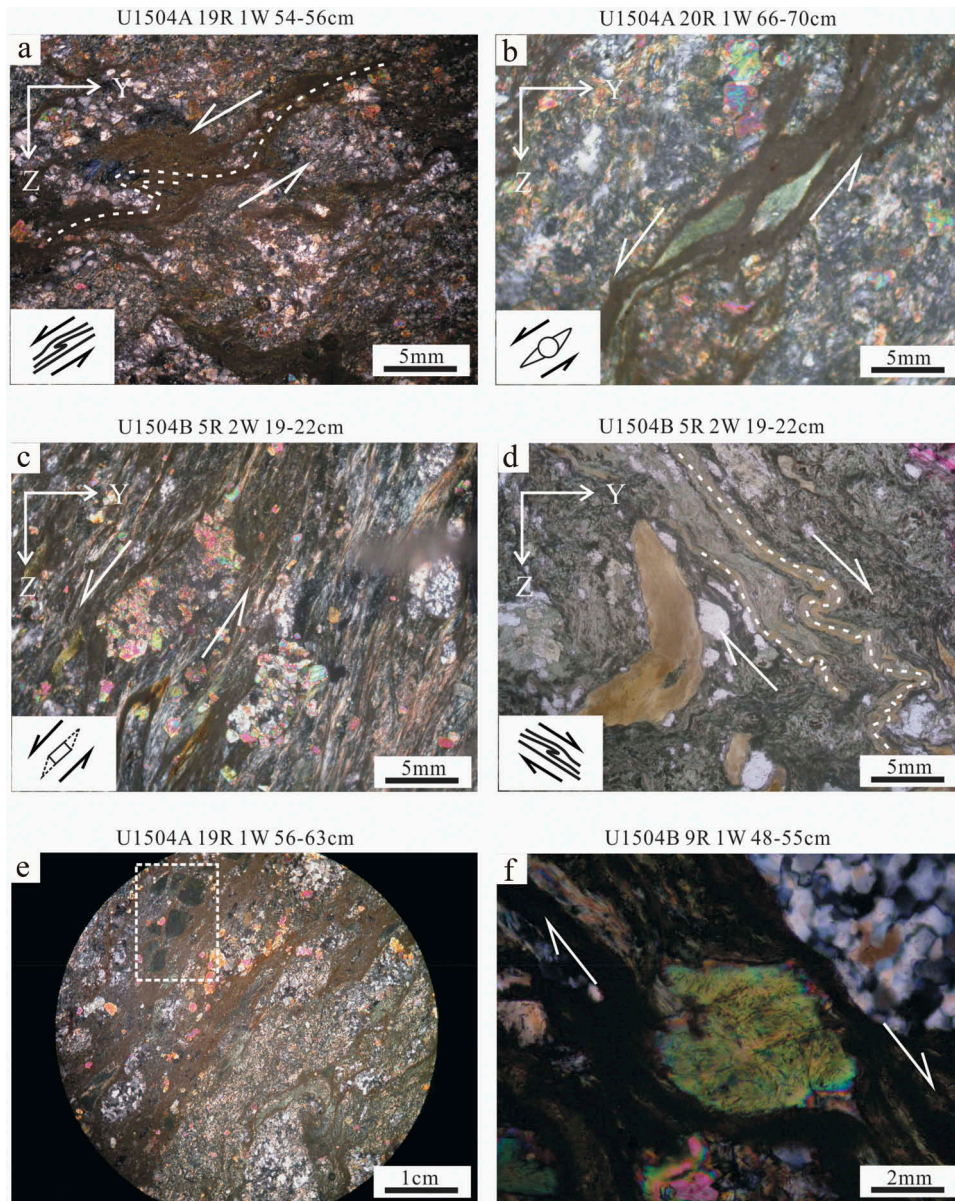


Figure 7. The microstructure of metamorphic rocks in Site U1504.

(a, d): Intrafolial folds; (b, c): Asymmetric rotational augen; (e): Mineral boudinage; (f): Pressure shadow. These microstructures indicate that the foliation is affected by normal shearing motion.

grained albite or metamorphic minerals (Figure 8(b,c)). Under the action of stress, some albite particles are obviously finely granulated into subgrains of albite that are slightly elongated in an orientation parallel to the foliation, with good development of deformation twins and undulatory extinction.

6. Discussion

6.1. Protolith reconstruction

Protolith reconstruction is an important part of the study of metamorphic rocks, and plays an important role in the

discussion of tectonic evolution stages and the restoration of regional geological development history. The methods of protolith reconstruction include petrography, mineralogy and geochemistry, but each method has some limitations and must be combined with geological background for a unified interpretation. During low grade metamorphism, the main chemical composition of the protolith basically does not change, so that the composition can be used to trace the chemical characteristics of the protolith. In the samples we studied, greenschist facies mylonite and chloritic breccia retain abundant clasts of the protolith, which can be reliably used to reconstruct the protolith.

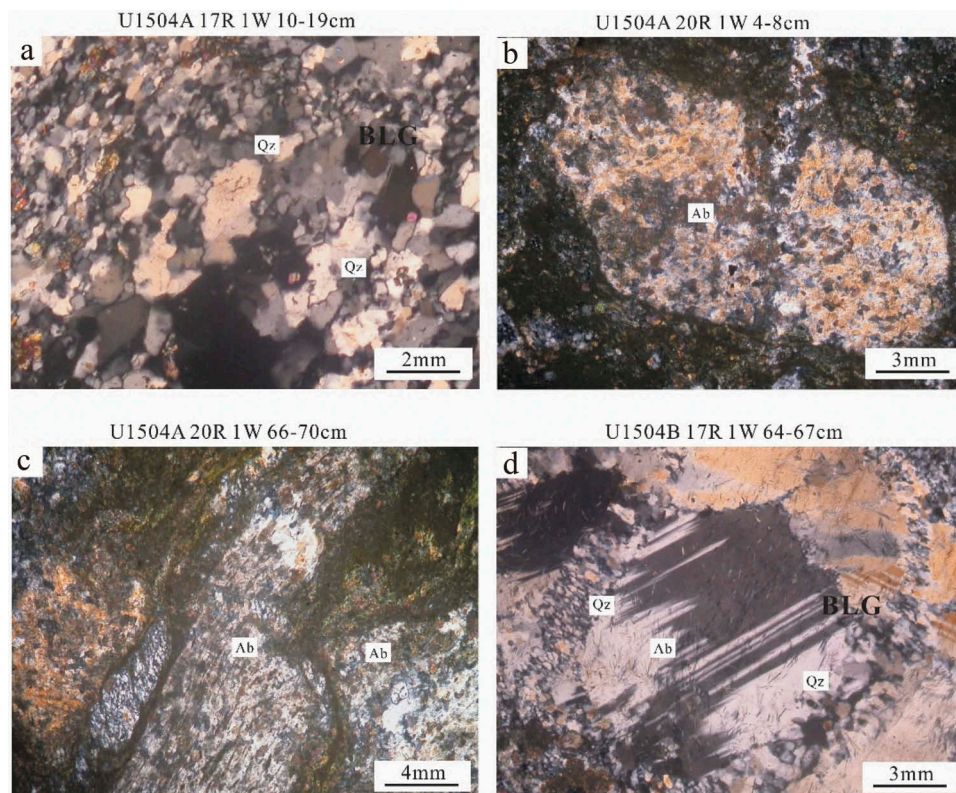


Figure 8. Microstructures observed in quartz and feldspar.

(a): Bulging recrystallization (BLG) of quartz. Recrystallized quartz grains from BLG zone are slightly elongated (ratio < 1:3) with a preferred orientation parallel to foliation, and have an irregular shape with serrated boundaries (0.1–0.5mm); (b): Residual dissolution structure of albite; (c): The residual feldspar crystals are often elongated and strongly fractured, and the fracture is filled with fine grained albite grains or metamorphic minerals; (d): Some recrystallized quartz grains developed along the periphery or within fissures of albite, forming an alteration zone around the albite grain. Qz: Quartz; BLG: Bulging recrystallization.

Therefore, geochemistry and petrography are combined to reconstruct the protolith in this paper.

IODP U1504 samples were analysed for major elements by XRF (Sun *et al.* 2018), from which some high quality data (Supplementary Table 4) were selected for geochemical analysis and protolith reconstruction in this study. The samples at Site U1504A and U1504B contain high MgO (4.55–10.46 wt%), Fe₂O₃ (7.93–15.04 wt%), Al₂O₃ (13.69–20.84 wt%), TiO₂ (1.05–2.94 wt%), and low SiO₂ (45.72–54.25 wt%) (Supplementary Table 4), which indicates that the protolith is related to mafic rocks. In addition, the samples of this study are similar to global MORBs, SCS MORBs (Zhang *et al.* 2018), IAB (SCICM) (Huang *et al.* 2013; Yan *et al.* 2014) and OIB (Yan *et al.* 2008; Zhang *et al.* 2017) in major element compositions (Figure 9), which further suggests that the protolith may be related to mafic magmatism in the SCS although its formation age is still unknown at present.

Greenschist facies mylonite and chloritization breccia retained many large clasts, which are close in composition to the protolith, including mafic igneous clasts and felsic terrigenous clasts. Mafic clasts are more abundant

than felsic ones. The mafic clasts are dominated by basalts, in which the albite and pyroxene are fine-grained and porphyritic texture is observed. The felsic clasts are small and show saussuritization. The crystals of feldspar and quartz are irregular in shape and underwent local dynamic recrystallization. Their protolith is presumed to be sedimentary rocks rather than felsic igneous rocks. These gravels are jumbled and distributed without apparent regularity, suggesting that the protoliths may be related to mafic magma and sedimentary rocks.

Combining geochemistry and petrography, we infer that the protolith corresponds to volcanic sedimentary rocks or basalts that interacted with sedimentary rocks.

6.2. Ductile deformation characteristics

6.2.1. The temperature of ductile deformation

It is quite often to constrain metamorphic temperatures and their geological significance based on empirically calibrated thermometers. But, it is difficult to estimate the temperature conditions of low-grade metamorphic rocks, such as our samples, due to the lack of suitable

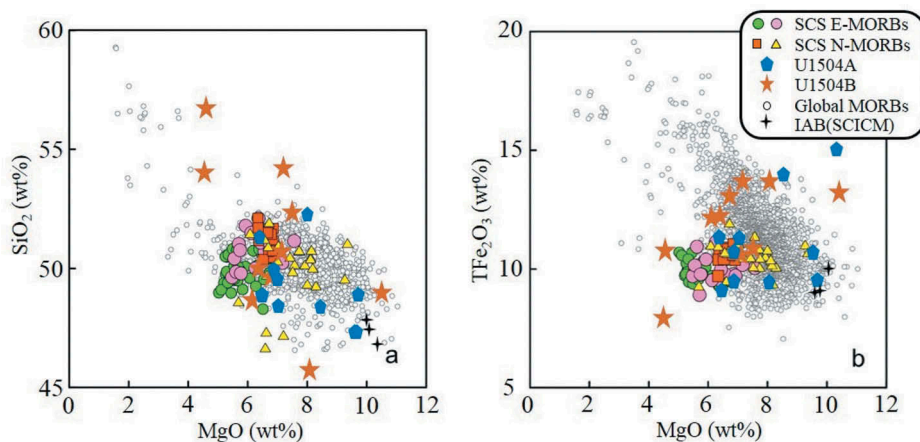


Figure 9. Plots of SiO_2 versus MgO , TFe_2O_3 versus MgO . Sources of data for comparison: the global mid-ocean ridge basalts (MORBs) (including East Pacific Rise, Indian ridge, Mid-Atlantic Ridge, Juan de Fuca Ridge, Chile ridge, Gakkel ridge), compiled and reported in Gale *et al.* (2013); SCS MORBs, compiled and reported in Zhang *et al.* (2018); Eocene island arc basalt (IAB) of the South China-Indochina continental margin (SCICM), compiled and reported in Huang *et al.* (2013).

thermometers. In some cases, the chlorite – quartz thermometers have been applied (Vidal *et al.* 2001; Lanari *et al.* 2014). However, such calculation always resulted in large errors ($\pm 50^\circ\text{C}$), moreover, in the case of the presence of fluids, the estimated temperature could be significantly lower than expected (Vidal *et al.* 2001). As such, this thermometer is not suitable for the studied samples because they were extensively affected by geofluids (Figures 3(b), 4(a), 6).

Alternatively, the metamorphic temperature could be inferred from microstructural characteristics and mineral assemblages. The temperature and pressure are two main controlling factors for the deformation of rocks and minerals, resulting in different microstructures and crystal forms (An 1986; Dai *et al.* 2012; Li *et al.* 2009). The deformation behaviours of quartz and feldspar, in particular, occupy the dominant position of earth's crust due to their stability in low to high pressure metamorphic conditions. The different microstructures and crystal forming conditions play an important role in the study of the dynamic processes of the crust. They are also the indicators of deformation temperature and pressure (Carter 1976; Wenk 1985, 1994). The microstructures of feldspar and quartz can be used to estimate the temperature of ductile deformation with an uncertainty of about 50°C (Cees *et al.* 2005). The temperature of BLG of quartz, brittle fracture and fine granulation of albite is about $300\text{--}400^\circ\text{C}$ (Frederico *et al.* 2010; Liang *et al.* 2015). On the other hand, because the mineral assemblage of the studied sample is chlorite + epidote + albite + quartz with no metamorphic biotite, the metamorphism related to the studied mylonite should be lower than the reaction of 'chlorite + feldspar = muscovite + biotite + quartz + H_2O ', which suggests an upper temperature limit of

approximately 400°C (Bucher and Frey 1994). Collectively, the intensively developed BLG of quartz, microscopic fractures and fine granulation of albite of the studied samples imply that the deformation temperature is between 300°C and 400°C (Figure 8). Therefore, the ductile deformation of the mylonites occurred under the metamorphic conditions of low- high greenschist facies, which is consistent with the petrographic characteristics (Figures 3 and 4).

Mesozoic-Cenozoic crust thinning of the continental margin of the SCS, associated with an elevated geothermal gradient ($37^\circ\text{C}/\text{km}$) (Tang *et al.* 2016) elevated the brittle-ductile transition zone up to relatively shallower crustal levels. In this regards, we speculate that the formation depth of the greenschist-facies mylonite is about 5-10km (lower to middle crust).

6.2.2. Finite deformation analysis

Finite strain analysis is an important way to quantitatively study the degree and type of deformation, which has been called the second nature of structural geology (White 1979; Hou 2018). To record the strain state of rocks, many methods are available; Wellman method, R_f/ϕ method, Heart to Heart method, Long and Short Axis method, Fry method and other methods have been widely used (Ramsay and Huber 1983; Fossen 2016; Hou 2018). The measurement of finite strain mainly uses spherical or nearly spherical markers such as ooids, beans, foraminifers, spherulites and holes in volcanic rocks, reduction spots in slates, and nearly isoaxial nodules and gravels. The gravel-bearing greenschist facies mylonites have randomly distributed gravels, which are nearly round and in

different sizes. They are ideal indicators of finite strain measurement. The Long and Short Axis method was chosen to study the finite deformation of gravel-bearing greenschist facies mylonites.

Firstly, we selected four samples with clear foliations and lineations to make oriented thin sections along the X-Y and Y-Z planes, and took microphotographs in positions rich in gravels. Then, over 30 felsic porphyroclasts were marked in the micrographs to measure the lengths of the long axis and the short axis. These were then used to calculate X/Y and Y/Z values respectively (Supplementary Table 2).

We plot the measured data on a Flinn diagram, which shows the uniform strain type, with Y/Z, X/Y of the strain ellipsoid as horizontal and vertical coordinates (logarithmic coordinates). Flinn's parameter $K = \ln(X/Y)/\ln(Y/Z)$. ' $0 < K < 1$ ' represents compressive strain and extrusion deformation; ' $1 < K < \infty$ ' represents elongation deformation and stretching strain; ' $K = 1$ ' represents plane strain. Measurement shows that the calculated k values are all slightly larger than 1.11 (Supplementary Table 3). The Flinn diagram (Figure 10) indicates that deformation behaviour of the greenschist facies mylonites are consistent. They all correspond to stretching strain, and the strain ellipsoid is a triaxial elongated ellipsoid. The simplest explanation for these observations is that the ductile foliation was developed in an extensional tectonic environment.

6.3. The formation mechanism of the greenschist facies mylonites

The greenschist facies mylonite samples were taken from the shoulder of the uplift in the OMH of the SCS. According to bathymetry, the uplift is a NE-trending ridge, with a large number of low-angle normal faults developed on its two flanks (Figure 11). These faults have opposite dip directions and small normal vertical displacement, with dip angles of about 45–60°. The basement surface is wavy with the graben and half-graben structures widely developed, suggesting a brittle extensional situation. There are also a large number of Cenozoic extensional structures developed in Baiyun Sag, Liwan Sag and Heshan Sag near the study area. Baiyun Sag is controlled by a series of continent-dipping detachment faults (Zhu *et al.* 2012; Ren *et al.* 2015), while Liwan Sag and Heshan Sag are controlled by a series of ocean-dipping detachment faults; Liwan Sag lies almost flat on a basement detachment belt (Ren *et al.* 2015), indicating that extensional structures are well developed in the transition zone of the SCS.

The foliations are well developed in the greenschist facies mylonites. The associated S-C fabric, asymmetric rotational

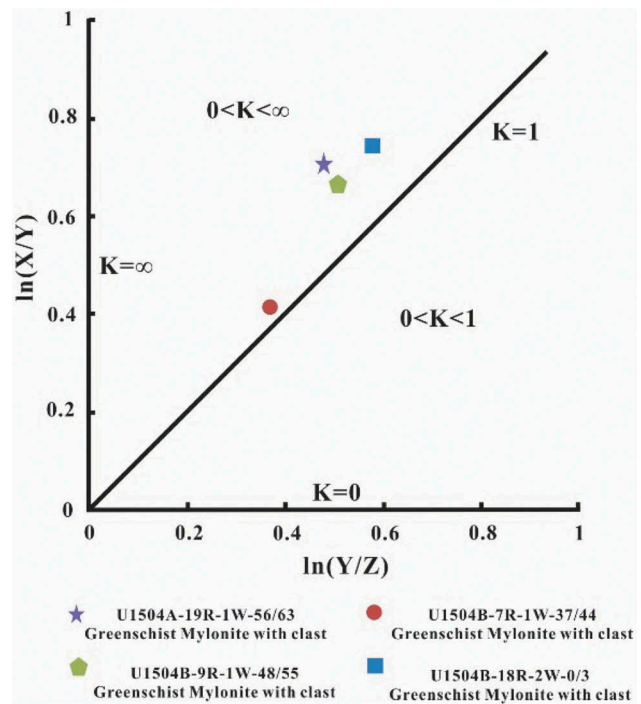


Figure 10. Flinn diagram of the greenschist facies mylonite.

Flinn diagram is a diagram showing the uniform strain type, with Y/Z, X/Y of the strain ellipsoid as horizontal and vertical coordinates (logarithmic coordinates). X, Y, Z are the principal strain axis of the strain ellipsoid; X parallel to the maximum elongation direction and called the maximum principal strain axis; Z parallel to the maximum compression direction and called the minimum principal strain axis; Y is somewhere between X and Z. Flinn's parameter $K = \ln(X/Y)/\ln(Y/Z)$; $0 < K < 1$ represent compressive strain and extrusion deformation; $1 < K < \infty$ represents elongation deformation and extensive strain. Measurement shows that the calculated K values are all slightly larger than 1.11, and indicates that deformation behaviours of the greenschist facies mylonites are deformed in extensive strain.

augen as well as the intrafolial folds (Figure 7), collectively suggest that the greenschist facies mylonites are associated with normal-sense ductile shearing, which is compatible with the regional structural patterns. In addition, the greenschist mylonite underwent two stages of deformation: the early ductile deformation that occurred in the ductile-brittle transition zone of the crust (at depth of ~5–10 km), forming widely developed mylonite layers; and the late brittle deformation developed in the shallow crustal layer, which led to the formation of rock fragmentation and cleavage. In summary, the greenschist mylonites underwent ductile to brittle deformation in the middle crust, then gradually were uplifted to a shallow crustal level in the process of regional extension, and finally were exposed to the surface (Figure 12). These features suggest that the mylonites may have been formed by ductile shearing during the development of regional extension.

Combining this evidence, we propose that the greenschist mylonite might have been formed by crustal exhumation after thick Mesozoic sediments were removed by significant extension. Located in the COT and covered with

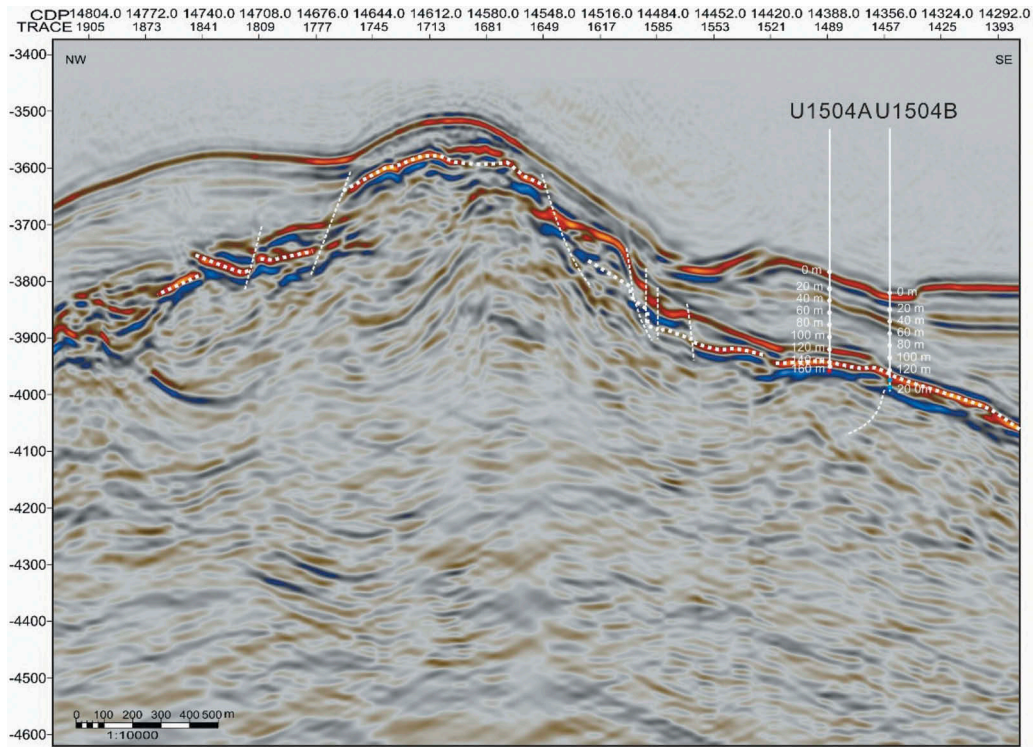


Figure 11. Seismic profiles of the study area. U1504A and B locate on the seaward slope of a basement high. Around the drilling site, ductile deformation with normal faults is observed.

The white dash lines are normal faults; the white dotted lines indicate the basement of Cenozoic sediments. All the numbers for the depth of the drill site are metre below seafloor.

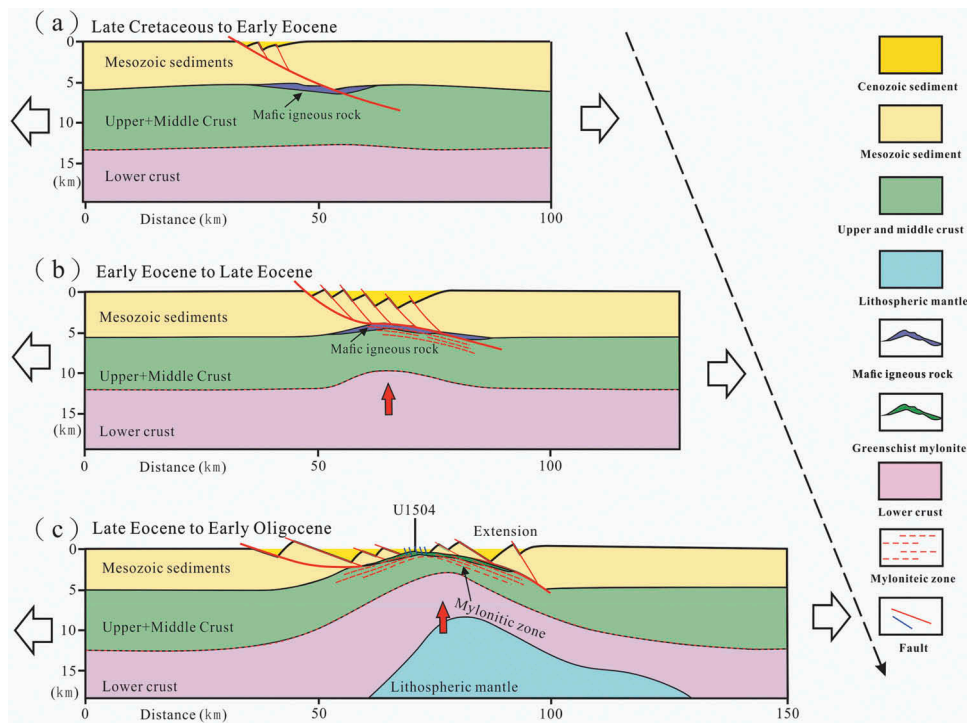


Figure 12. The model for greenschist facies mylonite formation in the northern continental margin of the SCS. In the Cenozoic, major extension and corresponding mantle upwelling in the northern continental margin caused ductile deformation of the crust in the COT and OMH, where middle crust or the lower part of the upper crust was exposed to the surface along the detachment fault. During crustal exhumation, greenschist mylonite might be formed in the ductile shear zone of the detachment fault. And, at this location in the COT and covered with thick Mesozoic sediments, the crust below U1504 might have been heated during extension and experienced ductile deformation.

thick Mesozoic sediments, the crust below U1504 might have been heated during extension and experienced a ductile deformation. Confirmation of this model awaits geochronology results on the timing of formation of the mylonites.

7. Conclusions

Based on the analysis of the petrography and microstructure of the rocks in Site U1504 in the northern continental margin of the SCS, combined with the seismic data, the following conclusions can be drawn:

- (1) The basement metamorphic rocks in Site U1504 can be divided into greenschist facies mylonites and chloritic breccia according to the lithologies. The greenschist facies mylonite is characterized by high-angle mylonitic foliations. It contains 10%–20% clasts, and the mineral assemblage is chlorite + epidote + albite ($Ab = 94.7\text{--}99.9$) + quartz, corresponding to greenschist facies. The mineral composition of the chloritic breccia is similar to that of the greenschist facies mylonite (albite: $Ab = 95.1\text{--}99.2$; pyroxene: $Wo_{42.3\text{--}45.4} En_{27.4\text{--}44.0} Fs_{23.5\text{--}11.5}$), showing weak mylonitic foliations. The chloritic breccia contains about 15–30% clasts, which are either mafic or felsic in composition.
- (2) The major element compositions of samples in Sites U1504 are similar to those of SCS MORBs, and petrographic features show that samples contain both mafic igneous and felsic sedimentary clasts. The protolith would be volcanic sedimentary rocks or basalts that interacted with sedimentary rocks.
- (3) The development of greenschist-facies mylonites is affected by the ductile shearing with a normal sense of shear at a ductile deformation temperature of about 300–400°C. Kinematic characteristics of greenschist-facies mylonites are consistent with the Cenozoic regional extensional structural features. The greenschist mylonite might have been formed during crustal exhumation as the Mesozoic sediments were removed due to high extension. Furthermore, the greenschist-facies mylonites underwent an early ductile deformation (at depth of 5–10 km) and a late brittle deformation (in the shallow crust), which is consistent with the gradual exhumation of these greenschist-facies mylonites from the deep crust to shallow crust.

Acknowledgments

This research was supported by the research team project of Guangdong Natural Science Foundation (2017A030312002), K.C.

Wong Education Foundation (GJTD-2018-13), South China Sea Deep Project (91628301), Guangdong Special Support Program to Y. D. J., CAS P.I.F.I. visiting professor project to J. M. S. (2019VMA0002) and the IODP-China Foundation.

Disclosure statement

No potential conflict of interest was reported by the authors.

Funding

This work was supported by the Natural Science Foundation of Guangdong Province [2017A030312002]; K.C. Wong Education Foundation [GJTD-2018-13]; IODP-China and South China Sea Deep Project [91628301]. CAS P.I.F.I. visiting professor project [2019VMA0002]; National Natural Science Foundation of China [41576070,41625007]; . This project used samples or data from the JOIDES Resolution Science Operator of the International Ocean Discovery Program, a large facility funded by the US National Science Foundation.

References

- An, L.J., 1986, The preliminary research on dynamic recrystallization and chemical transformations of feldspar in a mylonite zone: *Acta Petrologica Sinica*, v. 2, no. 3, p. 49–57. 99. [in Chinese with English abstract].
- Bucher, K., and Frey, M., 1994, *Petrogenesis of metamorphic rocks*: Heidelberg, Berlin, Springer-Verlag, 318p.
- Carter, L., 1976, Steady state flow of rocks: *Reviews of Geophysics and Space Physics*, v. 14, no. 3, p. 301–360.
- Cees, W., Passchier, Rudolph, A.J., and Trouw, 2005, *Microtectonics*: Berlin, Springer, 366.
- Childress, L., and the Expedition 368X Scientists, 2019, Expedition 368X preliminary report: South China Sea rifted margin: *International Ocean Discovery Program*. doi:10.14379/iodp.pr.368X.2019.
- Dai, Y.P., Zhu, Y.D., Wang, G.H., Zhang, L.C., TAO, H., Liu, Y., and Lv, Y.B., 2012, Microstructural characteristics of Anchanghe-Guanyinba fault zone in the Yangshan gold deposit of Gansu Province and their geological significance: *Geology in China*, v. 39, no. 3, p. 729–739. [in Chinese with English abstract].
- Fossen, H., 2016, *Structural Geology Second*: New York, USA, Cambridge University Press, p. 25–254.
- Frederico, M.F., Ginaldo, A.C.C., Rosa, M.S.B., and Kazuo, F., 2010, Quartz recrystallization regimes, c-axis texture transitions and fluid inclusion reequilibration in a prograde greenschist to amphibolite facies mylonite zone (Ribeira Shear Zone, SE Brazil): *Tectonophysics*, v. 485, p. 193–214. doi:10.1016/j.tecto.2009.12.014.
- Gale, A., Dalton, C.A., Langmuir, C.H., Su, Y., and Schilling, J.G., 2013, The mean composition of ocean ridge basalts: *Geochemistry, Geophysics, Geosystems*, v. 14, no. 3, p. 489–518. doi:10.1029/2012GC004334.
- Hou, Q.L., 2018, *Higher structural geology*: Beijing, Science Press, v. 2, 249p.
- Huang, X-L., Niu, Y.L., Xu, Y-G., Ma, J-L., Qiu, H-N., and Zhong, J-W., 2013. *Geochronology and geochemistry of*

- Cenozoic basalts from eastern Guangdong, SE China: constraints on the lithosphere evolution beneath the northern margin of the South China Sea. *Contributions to Mineralogy and Petrology*, v. 165, n.3, p. 437–455. doi:10.1007/s00410-012-0816-7
- Lanari, P., Wagner, T., and Vidal, O., 2014, A thermodynamic model for di-trioctahedral chlorite from experimental and natural data in the system MgO–FeO–Al₂O₃–SiO₂–H₂O: Applications to P–T sections and geothermometry: *Contributions to Mineralogy and Petrology*, v. 167, p. 1. doi:10.1007/s00410-014-0968-8.
- Larsen, H. C., Mohn, G., Nirrengarten, M., Sun, Z., Stock, J. M., Jian, Z., Klaus, A., Alvarez Zirikian, C. A., Boaga, J., Bowden, S. A., Briaies, A., Chen, Y., Cukur, D., Dadd, K. A., Ding, W., and Dorais, M. J., Ferré, E. C., Ferreira, F., Furusawa, A., Gewecke, A. J., Hinojosa, J. L., Höfig, T.W., Hsiung, K.-H., Huang, B., Huang, E., Huang, X.-L., Jiang, S., Jin, H., Johnson, B.G., Kurzawski, R. M., Lei, C., Li, B., Li, L., Li, Y., Lin, J., Liu, C., Liu, Z., Luna, A., Lupi, C., McCarthy, A.J., Mohn, G., Ningthoujam, L.S., Nirrengarten, M., Osono, N., Peate, D. W., Persaud, P., Qui, N., Robinson, C.M., Satolli, S., Sauermilch, I., Schindlbeck, J.C., Skinner, S.M., Straub, S.M., Zu, X., Tian, L., van der Zwan, F.M., Wan, S., Wu, H., Xiang, R., Yadav, R., Yi, L., Zhang, C., Zhang, J., Zhang, Y., Zhao, N., Zhong, G., and Zhong, L., 2018, Rapid transition from continental breakup to igneous oceanic crust in the South China Sea: *Nature Geoscience*, v. 11, p. 782–789. doi:10.1038/s41561-018-0198-1
- Li, F.C., Sun, Z., and Yang, H.F., 2018, Possible spatial distribution of the mesozoic volcanic arc in the present-day South China Sea continental margin and its tectonic implications: *Journal of Geophysical Research: Solid Earth*, N, v. 123, p. 6215–6235. doi:10.1029/2017JB014861.
- Li, S.Z., Suo, Y.H., Liu, X., Dai, L.M., Yu, S., Zhao, S.J., Ma, Y., Wang, X.F., and Cheng, S.X., 2012a, Basin Dynamics and basin groups of the South China Sea: *Marine Geology & Quaternary Geology*, v. 32, no. 6, p. 55–78. [in Chinese with English abstract]. doi:10.3724/SP.J.1140.2012.06055.
- Li, Z.X., Li, X.H., Chung, S.L., Lo, C.H., Xu, X., and Li, W.X., 2012b, Magmatic switch-on and switch-off along the south china continental margin since the Permian: Transition from an Andean-type to a western pacific-type plate boundary: *Tectonophysics*, v. 532-535, p. 271–290. doi:10.1016/j.tecto.2012.02.011.
- Liang, C.Y., Liu, Y.J., Neubaue, F., Wei, J., Genser, J., Li, W.M., Li, W., Han, G., Wen, Q.G.B., Zhao, Y.L., and Cai, L.B., 2015, Structural characteristics and LA–ICP–MS U–Pb zircon geochronology of the deformed granitic rocks from the Mesozoic Xingcheng–Taili ductile shear zone in the North China Craton: *Tectonophysics*, v. 650, p. 80–103. doi:10.1016/j.tecto.2014.05.010.
- Luan, X.W., and Zhang, L., 2009, Tectonic evolution modes of South China Sea: Passive spreading under complex actions: *Marine Geology & Quaternary Geology*, v. 29, no. 6, p. 59–74. [in Chinese with English abstract]. doi:10.3724/SP.J.1140.2009.06059.
- Ramsay, J.G., and Huber, M.I., 1983, *The technique of modern structural geology*: London, Academic Press, v. 1, 307p.
- Ren, J.Y., Pang, X., Lei, C., Yuan, L.Z., Liu, J., and Yang, L.L., 2015, Ocean and continent transition in passive continental margins and analysis of lithospheric extension and breakup process: Implication for research of the deepwater basins in the continental margins of South China Sea: *Earth Science Frontiers*, v. 22, no. 1, p. 102–114. [in Chinese with English abstract].
- Seton, M., Flament, N., Whittaker, J., Müller, R., Dietmar, G.M., and Bower, D.J., 2015, Ridge subduction sparked reorganization of the Pacific plate-mantle system 60–50 million years ago: *Geophysical Research Letters*, v. 42, no. 6, p. 1732–1740. doi:10.1002/2015GL063057.
- Sun, Z., Jian, Z., Stock, J.M., Larsen, H.C., Klaus, A., Alvarez Zirikian, C.A., Boaga, J., Bowden, S.A., Briaies, A., Chen, Y., Cukur, D., Dadd, K.A., Ding, W., Dorais, M.J., Ferré, E.C., Ferreira, F., Furusawa, A., Gewecke, A.J., Hinojosa, J.L., Höfig, T. W., Hsiung, K.-H., Huang, B., Huang, E., Huang, X.L., Jiang, S., Jin, H., Johnson, B.G., Kurzawski, R., Lei, M.C., Li, B., Li, L., Li, Y., Lin, J., Liu, C., Liu, Z., Luna, A., Lupi, C., McCarthy, A.J., Mohn, G., Ningthoujam, L.S., Nirrengarten, M., Osono, N., Peate, D.W., Persaud, P., Qui, N., Robinson, C.M., Satolli, S., Sauermilch, I., Schindlbeck, J.C., Skinner, S.M., Straub, S.M., Zu, X., Tian, L., van der Zwan, F.M., Wan, S., Wu, H., Xiang, R., Yadav, R., Yi, L., Zhang, C., Zhang, J., Zhang, Y., Zhao, N., Zhong, G., and Zhong, L., 2018, Expedition 367/368 methods, in Sun, Z., Jian, Z., Stock, Larsen, J.M., Klaus, H.C., and Alvarez Zirikian, A. C.A., and the Expedition 367/368 Scientists, eds., *South China Sea rifted margin proceedings of the international ocean discovery program, 367/368*: CollegeStation, TX, International Ocean Discovery Program, 68p. doi:10.14379/iodp.proc.367368.102.2018.
- Sun, Z., Stock, J., Jian, Z., McIntosh, K., Alvarez Zirikian, C.A., and Klaus, A., 2016, Expedition 367/368 scientific prospectus, South China Sea rifted margin: CollegeStation, TX, International ocean discovery program, 57p. doi:10.14379/iodp.sp.367368.2016.
- Sutra, E., and Manatschal, G., 2012, How does the continental crust thin in a hyperextended rifted margin? Insights from the Iberia margin: *Geology*, v. 40, no. 2, p. 139–142. doi:10.1130/G32786.1.
- Sutra, E., Manatschal, G., Mohn, G., and Unternehr, P., 2013, Quantification and restoration of extensional deformation along the Western Iberia and Newfoundland rifted margins: *Geochemistry, Geophysics, Geosystems*, v. 14, no. 8, p. 2575–2597. doi:10.1002/ggge.20135.
- Tang, X.Y., Huang, S.P., Yang, S.C., Jang, G.Z., and Hu, S.B., 2016, Correcting on logging-derived temperatures of the Pearl River Mouth Basin and characteristics if its present temperature field: *Chinese Journal of Geophysics*, v. 59, p. 2911–2921. [in Chinese with English abstract].
- Taylor, B., and Hayes, D.E., 1983, *Origin and history of the South China Sea basin*: Washington Dc, American Geophysical Union Geophysical Monograph, Vol. 27, p. 23–56.
- Vidal, O., Parra, T., and Trotet, F., 2001, A thermodynamic model for Fe–Mg aluminous chlorite using data from phase equilibrium experiments and natural polytic assemblages in the 100–600 °C, 1–25 kbar P–T range: *American Journal of Science*, v. 301, p. 557–592. doi:10.2475/ajs.301.6.557.
- Wang, P.X., 2012, Tracing the life history of a marginal Sea —On the ‘South China Sea Deep’ Research Program: *Chinese Science Bulletin*, v. 57, no. 20, p. 1807–1826. [in Chinese with English abstract]. doi:10.1007/s11434-012-5087-1.
- Wenk, H.R., 1985, *Preferred orientation in deformed metal and rocks: an introduction to modern texture analysis*: London, Academic Press.

- Wenk, H.R., 1994, Preferred orientation patterns in deformed quartzites: *Reviews in Mineralogy and Geochemistry*, v. 29, p. 177–208.
- White, S.H., 1979, Large strain deformation: Report on a tectonic studied group discussion meeting held at Imperial College, Longdon on 14 November 1979: *Journal of Structural Geology*, v. 1, no. 4, p. 333–339. doi:10.1016/0191-8141(79)90008-7.
- Yan, Q.S., Shi, X.F., and Castillo, P.R., 2014, The late Mesozoic–Cenozoic tectonic evolution of the South China Sea: A petrologic perspective: *Journal of Asian Earth Sciences*, v. 85, p. 178–201. doi:10.1016/j.jseaes.2014.02.005.
- Yan, Q.S., Shi, X.F., Wang, K.S., Bu, W.R., and Xiao, L., 2008, Major element, trace element, Sr–Nd–Pb isotopic studies of Cenozoic alkali basalts from the South China Sea: *Sci: Science in China Series D: Earth Sciences*, v. 51, p. 550–566. doi:10.1007/s11430-008-0026-3.
- Yao, B.C., 1996, Tectonic evolution of the South China Sea in Cenozoic [J]: *Marine Geology & Quaternary Geology*, v. 16, no. 2, p. 1–13. [in Chinese with English abstract].
- Zhang, G.L., Chen, L.H., Jackson, M.G., and Hofmann, A.W., 2017, Evolution of carbonated melt to alkali basalt in the South China Sea: *Nature Geoscience*, v. 10, p. 229–235. doi:10.1038/ngeo2877.
- Zhang, G.L., Lou, Q., Zhao, J., Jackson, M.G., Gou, L.S., and Zhong, L.F., 2018, Geochemical nature of sub-ridge mantle and opening dynamics of the South China Sea: *Earth and Planetary Science Letters*, v. 489, p. 145–155. doi:10.1016/j.epsl.2018.02.040.
- Zhang, L., 2012, Tectonic evolution of the South China Sea and a Numerical modeling [Ph. D thesis]: Beijing, Graduate University of Chinese Academy of Sciences, 188 p. [in Chinese with English abstract].
- Zhou, Z.C., 2018, The Cenozoic crustal thinning and development of hyper-extended rift system in the northern South China Sea [Ph. D thesis]: Beijing, China University of Geosciences, 174 p.
- Zhu, J.J., Qiu, X.L., Kopp, H., Sun, Z.X., Ruan, A., Sun, J.L., and Wei, X.D., 2012, Shallow anatomy of a continent-ocean transition zone in the northern South China Sea from multi-channel seismic data: *Tectonophysics*, N, v. 554–557, p. 18–29. doi:10.1016/j.tecto.2012.05.027.